Construction and Building Materials xxx (xxxx) xxx

Contents lists available at ScienceDirect

Construction and Building Materials

journal homepage: www.elsevier.com/locate/conbuildmat

Stress-strain behavior of FRP-confined concrete containing recycled concrete lumps

J.K. Zhou [a,b], Guan Lin [b,*], J.G. Teng [b]

[a] School of Civil and Transportation Engineering, Guangdong University of Technology, Guangzhou 510006, China
[b] Department of Civil and Environmental Engineering, The Hong Kong Polytechnic University, Hong Kong, China

HIGHLIGHTS

- Sixteen FRP-confined compound concrete columns containing RCLs were tested.
- The inclusion of RCLs reduces the compressive strength of unconfined concrete.
- FRP confinement can significantly enhance the performance of compound concrete.
- The behavior of FRP-confined compound concrete can be predicted closely by an existing model.

ARTICLE INFO

Article history:
Received 19 March 2020
Received in revised form 31 August 2020
Accepted 12 September 2020
Available online xxxx

Keywords:
Fiber reinforced polymer (FRP)
Recycled concrete lumps (RCLs)
Compound concrete
FRP tubes
Confinement
Stress-strain behavior

ABSTRACT

A novel method to recycle concrete is to crush demolition concrete into large pieces and then to directly mix the resulting recycled concrete lumps (RCLs) with fresh concrete to produce a new kind of recycled concrete referred to as "compound concrete". This method avoids the complexity of recycling concrete into aggregates and enables the achievement of a higher recycling ratio and a lower recycling cost. However, due to the large sizes of RCLs and the weak interfaces between fresh concrete and RCLs, compound concrete is much more heterogeneous than normal concrete. A new technique has recently been explored to improve the properties of such compound concrete, in which the compound concrete is provided with a substantial amount of confinement from an external fiber-reinforced polymer (FRP) confining tube. This paper presents the results of an experimental program of axial compression tests on compound concrete-filled FRP tubular columns in which the FRP tubes were prefabricated using the wet lay-up method with fibers only in the hoop direction. The tubes had a negligible axial stiffness, which allows the stress-strain behavior of FRP-confined compound concrete to be clearly revealed. The test results show that, when a significant level of FRP confinement is provided, the behavior of FRP-confined compound concrete is similar to that of FRP-confined normal concrete with a strength equal to that of the fresh concrete. An existing stress-strain model previously developed for FRP-confined normal concrete is evaluated in the paper using the test results of FRP-confined compound concrete.

1. Introduction

A typical method of using demolition concrete is to recycle it into coarse and fine aggregates (normally only coarse aggregate which is referred to as recycled coarse aggregate or RCA) which are then used in making new concrete, and such new concrete is referred to as recycled aggregate concrete (RAC) . The research and application of RAC have received great attention in many countries [1–10]. The existing research has concluded that the presence of RCA leads to inferior concrete performance, including reductions in stiffness and strength as well as increases in shrinkage and creep when compared with its natural aggregate concrete counterpart [4,11].

In addition to the inferior performance of RAC, the recycling of demolition concrete into RCA involves complicated and uneconomic processes of crushing, screening, and cleaning, which limit the wide application of RAC. Recently, Wu et al. [12] proposed a new concept in which demolition concrete is crushed into large pieces and the resulting recycled concrete lumps (RCLs) are directly mixed with fresh concrete to produce a new kind of recycled concrete which has been referred to as "compound concrete" [13,14]. This novel recycling method substantially simplifies the recycling process and reduces the recycling cost. In addition, the

* Corresponding author.
E-mail address: guanlin@polyu.edu.hk (G. Lin).

https://doi.org/10.1016/j.conbuildmat.2020.120915
0950-0618/

recycling ratio (the ratio between the weight of the recycled portion and the total weight of the old concrete) can be significantly increased compared with that of RAC. The feasibility of this new recycling method has been demonstrated by Wu's research group through testing structural members made of such compound concrete (e.g, [15–21]), including: (1) axial compression tests on concrete columns containing RCLs [15,16]; (2) axial compression tests on compound concrete-filled steel tubular (CCFST) columns [17]; (3) eccentric compression tests on slender CCFST columns [18]; and (4) cyclic lateral loading tests on square CCFST columns [19]. In addition to the structural performance of members made of compound concrete, other aspects related to compound concrete, such as the size effect of concrete specimens containing RCLs [15] and creep behavior of compound concrete in steel tubular columns [20], have also been investigated. Two real-world construction projects in Guangzhou, China, involving the use of CCFST columns, have also been reported [21].

The above studies, however, have shown that the presence of RCLs leads to reductions in the performance of compound concrete compared with normal concrete, due to at least the following two issues: (1) compound concrete is much more heterogeneous than normal concrete due to the large sizes of RCLs, especially when the difference in strength between the RCLs and the fresh concrete is relatively large; (2) the interfaces between the fresh concrete and the RCLs may exhibit weaknesses. Wu et al. [19] found that the compressive strength (ultimate stress) of compound concrete, as well as the load-carrying capacity of CCFST columns, decreases as the RCL mix ratio (i.e., the weight ratio between the RCLs and the resulting compound concrete) increases. In addition, compound concrete tends to have premature cracking due to interfacial weaknesses, which has a detrimental durability effect on the internal steel reinforcement. An attractive approach to reduce or eliminate the weaknesses caused by the use of RCLs is to use compound concrete as the filler material in tubular columns, where the tube confines the compound concrete and isolates it from direct exposure to the service environment. Wu's research group has explored the use of compound concrete in concrete-filled steel tubular columns [17–19,22]. They have found that the detrimental effects of RCLs can be eliminated or minimized only when a stocky steel tube (i.e., one with a small diameter or width-to-thickness ratio) is used. This is because the confinement provided by a steel tube is limited due to: (1) the steel tube in axial compression expands more than the compound concrete core during the early stage of loading; (2) the steel tube yields once the concrete has developed macro-cracking.

More recently, Teng et al. [13,14] proposed the combination of fiber-reinforced polymer (FRP) tubes with compound concrete to form FRP-confined compound concrete (FCCC) columns. In such FRP tubes, the fibers are oriented close to the hoop direction of the tube and thus the tubes are strong and stiff in the hoop direction mainly to provide confinement and shear resistance to FCCC columns [23,24]. The use of FRP tubes rather than steel tubes has the following advantages: (1) better confinement as the FRP tube has negligible axial resistance/stiffness so its lateral dilation is much smaller than the concrete core right from the beginning of loading; (2) better durability as the FRP tube has excellent corrosion resistance. Teng et al. [14] carried out the first experimental study on the compressive behavior of FCCC columns under axial compression. In their tests, glass FRP (GFRP) tubes formed using the filament winding process were used. Their study revealed an additional but very important benefit offered by the FRP tube: with the confinement provided by the FRP tube, the compound concrete could exhibit a stress-strain behavior close to that of the fresh concrete which had a much higher strength than the old concrete from which the RCLs were made. This observation means that FRP confinement can effectively eliminate the weakness in compressive strength caused by the use of RCLs. More importantly, this observation means that although old concrete generally has a comparatively low compressive strength, the strength of the new compound concrete is not limited or significantly affected by this low strength; instead, by using high strength fresh concrete with RCLs, the resulting compound concrete can be expected to be almost as strong as the fresh concrete under an appropriate level of confinement.

The study conducted by Teng et al. [14] suggests that much more research needs to be conducted to develop a comprehensive understanding of the behavior of FRP-confined compound concrete. In addition, since filament-wound FRP tubes were used in the previous study [14], the significant axial stiffness of the FRP tubes (although the fibers were oriented close to the hoop direction) led to some uncertainty in understanding the confinement mechanism in FRP-confined compound concrete [37]. As a result, a new experimental program was carried out in the present study, in which carbon FRP (CFRP) tubes prefabricated via the wet lay-up method with fibers oriented only in the hoop direction were used. These tubes had a negligible axial stiffness and provided great flexibility in the choice of confinement levels, which allowed the stress-strain behavior of FRP-confined compound concrete to be clearly revealed. The experimental program consisted of 36 columns (among which 16 were FCCC columns) subject to monotonic axial compression. The experimental variables included the mix ratio of RCLs, the CFRP tube thickness, and the compressive strength of fresh concrete. An existing stress–strain model previously developed for FRP-confined normal concrete [i.e., Jiang and Teng's model] [25] was evaluated using the test results. In the practical applications of FCCC columns, however, filament-wound FRP tubes should still be used.

2. Experimental program

2.1. Recycled concrete lumps (RCLs)

The RCLs were produced from standard concrete cylinders with a diameter of 150 mm and a height of 300 mm which had been tested under axial compression. The concrete was prepared with ordinary portland cement, river sand, superplasticizer (S.P.), and crushed granite coarse aggregate with a maximum nominal size of 20 mm. The concrete cylinders had been cast and cured at room temperature for at least 28 days before the crushing operation. Only RCLs passing a test sieve of 100 mm mesh size but retained on a test sieve of 60 mm mesh size (i.e., RCLs with a minimum dimension between 60 mm and 100 mm) were selected for inclusion in the compound concrete. The number of RCLs with a minimum dimension of 80–100 mm was around twice the number of RCLs with a minimum dimension of 60–80 mm. The compressive strength of RCLs was assumed to be equal to the compressive strength of the corresponding series of concrete cylinders used to produce the RCLs. The average compressive cylinder strengths for the two series of concrete cylinders (Series I and Series II) were found to be 33.1 MPa and 41.8 MPa, respectively. The water absorptions in mass and density of the two series of RCLs in the saturated surface-dry condition were almost the same and they were measured to be 4.53% and 2.36 g/cm^3 (Table 1), respectively,

Table 1
Material properties of RCLs.

Water absorption	Density (g/cm^3)	Cylinder compressive strength of Series I (MPa)	Cylinder compressive strength of Series II (MPa)
4.53%	2.36	33.1	41.8

according to BS 812 [26]. Fig. 1 shows a photo of three RCLs with the typical highly irregular surfaces, where the mortar of the old concrete and the coarse aggregate can be clearly seen.

2.2. Specimen details

A total of thirty-six columns in two series were prepared and tested. Table 2 shows the key parameters of the columns. All the columns had a diameter of 200 mm and a height of 400 mm for the concrete core, leading to an RCL-to-specimen size ratio (i.e., the ratio between the maximum dimension of RCLs and the diameter of the circular concrete core) of 0.5. Wu et al. [15] reported that the RCL-to-specimen size ratio has limited influence on the behavior of compound concrete (the range of RCL-to-specimen size ratio examined in their study was from 0.1 to 0.6). Therefore, only one specimen size (i.e., 200 mm × 400 mm) was used in the present study. The specimens were divided into two series based on the compressive strength of RCLs. In Series I, the target compressive strength of fresh concrete (40 MPa) was similar to and slightly higher than that of RCLs (33.1 MPa), while in Series II the target strength of fresh concrete (60 MPa) was much higher than that of RCLs (41.8 MPa). The strength of fresh concrete in Series II was designed to be much higher than that of RCLs as RCLs in practice are generally obtained from old structures with a low concrete strength. Crushed granite coarse aggregate with a maximum nominal size of 20 mm was also used in the fresh concrete. Both series included three different confinement levels (i.e., 0-ply, 2-ply, and 3-ply CFRP tubes) and three different RCL mix ratios as the key test variables. For each column configuration, two duplicate (nominally identical) specimens were tested. Each column was given a name in the form of CX-RY-TZ-1,2 where X represents the target strength of fresh concrete, Y indicates the RCL mix ratio (in percentage), and Z represents the number of plies of the CFRP tube. The final number 1 or 2 is to differentiate two duplicate specimens. The specimens in each series were cast in three batches corresponding to three different thicknesses of the CFRP tubes. For each batch, three standard concrete cylinders were also cast and tested before (within one weak) the testing of column specimens to obtain the fresh concrete properties. The compressive strength (f'_{co}) and the axial strain at peak stress (ε_{co}) of fresh concrete in each batch are listed in Table 2. The readings of two LVDTs (linear variable differential transformers) covering a mid-height region of 150 mm were used to obtain the axial strains.

Fig. 1. Recycled concrete lumps (RCLs).

2.3. FRP tubes

All the CFRP tubes were prefabricated manually using the wet lay-up method by wrapping an epoxy impregnated carbon fiber sheet around a bakelite mold in the hoop direction (Fig. 2). Before the wrapping of the fiber sheet, a plastic film was used to cover the external surface of the mold to ensure that demolding would be easy and the internal surface of the CFRP tube would be smooth. A 200-mm overlapping zone of the carbon fiber sheet was adopted. Each end of the CFRP tube was strengthened with an additional 25-mm-wide CFRP strip to ensure that failure of an FCCC column would not occur near the two ends of the column (Fig. 2c). FRP tubes on the mold were cured in laboratory for 48 h before demolding. Three one-ply flat CFRP coupons were also fabricated and tested to determine the properties of the CFRP in accordance with ASTM D3039 [27]. The average rupture strain, tensile strength, and elastic modulus were found from the tensile tests to be 1.83%, 4810 MPa, and 246 GPa, respectively, based on a nominal thickness of 0.167 mm per layer. The elastic modulus was determined from the linear portions of the tensile stress-strain curves of the FRP coupons with tensile strains between 0.1% and

Table 2
Specimens details.

Series	Specimen	Fresh concrete cylinder strength (MPa)	Compressive strain at peak stress	RCL cylinder strength (MPa)	CFRP tube	RCL mix ratio (%)
Series I	C40-R0-T0-1,2	41.7	0.00301	–	0	0
	C40-R15-T0-1,2			33.1		15
	C40-R30-T0-1,2			33.1		30
	C40-R0-T2-1,2	39.3	0.00305	–	2-ply	0
	C40-R15-T2-1,2			33.1		15
	C40-R30-T2-1,2			33.1		30
	C40-R0-T3-1,2	38.8	0.00312	–	3-ply	0
	C40-R15-T3-1,2			33.1		15
	C40-R30-T3-1,2			33.1		30
Series II	C60-R0-T0-1,2	64.0	0.00312	–	0	0
	C60-R15-T0-1,2			41.8		15
	C60-R30-T0-1,2			41.8		30
	C60-R0-T2-1,2	63.6	0.00305	–	2-ply	0
	C60-R15-T2-1,2			41.8		15
	C60-R30-T2-1,2			41.8		30
	C60-R0-T3-1,2	62.0	0.00286	–	3-ply	0
	C60-R15-T3-1,2			41.8		15
	C60-R30-T3-1,2			41.8		30

(a) Bakelite mold

(b) Wrapping of a carbon fiber sheet

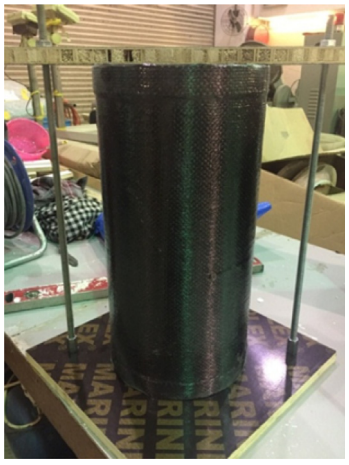

(c) CFRP tube after curing

Fig. 2. Preparation of CFRP tubes.

0.3% in accordance with ASTM D3039 [27]. The tensile stress-strain curves generally followed the linear curve of the elastic modulus until the tensile strain reached around 1.3% (a value that is not far from the average FRP hoop rupture strain measured in the FCCC column tests), after which the stress–strain curves exhibited a small degree of nonlinearity, which explains why the measured rupture strain is smaller than the tensile strength divided by the elastic modulus. In the subsequent theoretical analysis, only the elastic modulus needed to be used to calculate the FRP confining pressure.

2.4. Fabrication of column specimens

All the RCLs were placed in water for 24 h and then dried using dry towels to ensure a saturated surface-dry condition before being mixed with fresh concrete. For all the FCCC columns or FRP-confined concrete columns without RCLs, the CFRP tubes, which served as the formwork, were first fixed on two wooden plates before concrete casting (Fig. 2c). During the casting process, a thin layer of fresh concrete was first poured to the bottom of the tube. RCLs and fresh concrete were then alternately added into the tube. In the meantime, the tube was put on a vibration table to achieve good compaction of the compound concrete. For the unconfined column specimens, PVC tubes instead of CFRP tubes were used as formwork for concrete casting. After curing at room temperature for 28 days, the PVC tubes were removed from the specimens.

2.5. Test set-up and instrumentation

For each FRP-confined specimen, eight horizontal strain gauges (gauge length = 20 mm) were evenly distributed around the circumference of the mid-height section to measure the hoop strains (three of these hoop strain gauges were installed in the overlapping region) and four axial strain gauges (gauge length = 20 mm) were attached at 90° apart to measure the axial strains (Fig. 3a). In addition, four LVDTs were installed in a mid-height region of 210 mm at 90° apart to enable the measurement of axial shortenings of the specimen (Fig. 3a). These LVDTs were installed onto a steel frame which was attached to the specimen (Fig. 3b). For each unconfined column specimen, four axial strain gauges (gauge length = 100 mm) and four horizontal strain gauges (gauge length = 50 mm) were attached at 90° apart at the mid-height to measure the axial strains and the hoop strains, respectively; four LVDTs were also installed to cover a mid-height region of 210 mm at 90° apart to measure the axial shortenings.

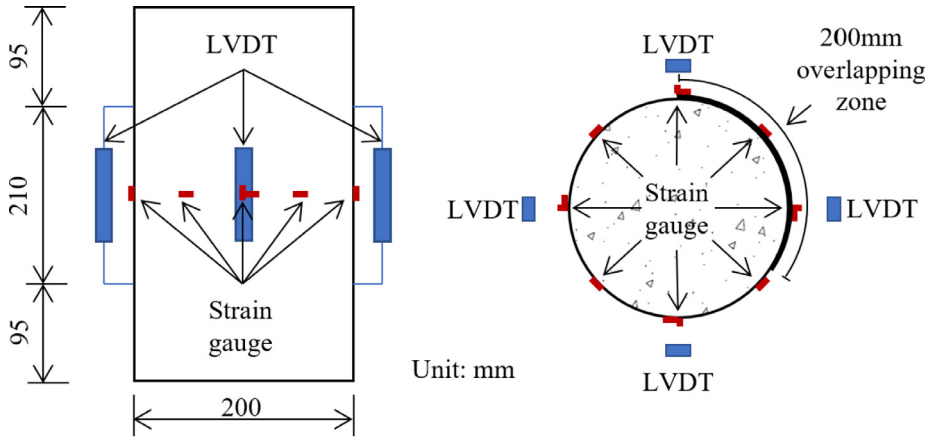

(a) Layout of LVDTs and strain gauges

(b) Test set-up

Fig. 3. Instrumentation and test set-up for FCCC columns.

All specimens in Series I were tested at a rate of 0.24 mm/min with displacement control on an MTS machine (capacity = 4600 kN), while all specimens in Series II were tested on a testing frame with a larger capacity (10,000 kN). A displacement-controlled loading rate of 0.30 mm/min was adopted for specimens in Series II.

3. Test results and discussions

3.1. General observations

All the unconfined concrete specimens failed by concrete crushing with visible cracks (Fig. 4). The presence of RCLs did not seem to have an obvious effect on their failure mode. The failure modes of the two series of specimens are slightly different: Series I specimens failed in a more gradual process with cracks of small width developing gradually, while Series II specimens generally failed in a more brittle manner with the formation of one major crack. The difference in the failure mode was mainly caused by the strength difference between the fresh concrete and the RCLs in the two series. The key experimental results of these specimens, including the compressive strength f'_{co} and the axial strain at peak stress ε_{co} are summarized in Table 3. The axial strains were obtained from the mid-height LVDT readings. It is obvious that the inclusion of RCLs reduced considerably the strength of unconfined concrete, and the reduction increased with the RCL mix ratio. For Series I specimens, the mix ratios of 15% and 30% led to decreases of 13.1% and 20.5%, respectively, in the compressive strength. For Series II specimens, the corresponding reductions in the compressive strength are 14.4% and 25.9%, respectively. It can be seen that Series II specimens had larger percentage reductions in compressive strength than the corresponding specimens in Series I since the strength difference between the RCLs and the fresh concrete was larger in Series II. Note that the reduction in the compressive strength of unconfined concrete was mainly caused by the lower strength of RCLs than that of the fresh concrete. If the strength of the RCLs is larger than that of the fresh concrete, a larger compressive strength than the fresh concrete can be developed for the compound concrete [14].

Fig. 5 shows the surface of fracture of an unconfined concrete column containing RCLs. The interfaces between the fresh concrete and the RCLs are also indicated in the figure. It appears that the RCLs were well embedded in the fresh concrete and no visible cracking or damage occurred at the interfaces between the fresh concrete and the RCLs. In addition, it was observed that the RCLs were generally cut through by the fracture paths of the specimen, which is different from the failure of normal concrete where the fracture paths generally go around the aggregate pieces.

Note that for specimens C40-R0-T2, C40-R15-T2, and C40-R30-T2, the results of one of the two duplicate specimens have been

(a) C40-R0-T0 (b) C40-R15-T0 (c) C40-R30-T0

(d) C60-R0-T0-1 (e) C60-R15-T0-1 (f) C60-R30-T0-1

Fig. 4. Unconfined concrete specimens after test.

Table 3
Key experimental results of unconfined concrete column specimens.

Series	Specimen	f'_{co} (MPa)	Average f'_{co} (MPa)	ε_{co}	Average ε_{co}
Series I	C40-R0-T0-1	42.1	42.0	0.00305	0.00312
	C40-R0-T0-2	41.9		0.00319	
	C40-R15-T0-1	35.9	36.5	0.00292	0.00300
	C40-R15-T0-2	37.1		0.00308	
	C40-R30-T0-1	33.3	33.3	0.00307	0.00300
	C40-R30-T0-2	33.3		0.00292	
Series II	C60-R0-T0-1	65.2	66.2	0.00318	0.00334
	C60-R0-T0-2	67.1		0.00350	
	C60-R15-T0-1	56.6	56.6	0.00280	0.00296
	C60-R15-T0-2	56.6		0.00311	
	C60-R30-T0-1	50.0	49.0	0.00249	0.00266
	C60-R30-T0-2	48.0		0.00282	

excluded because an outdated resin was used in fabricating the CFRP tubes, leading to premature debonding failure in the overlapping zone of these CFRP tubes. All the remaining FCCC specimens and FRP-confined normal concrete specimens failed suddenly by the rupture of CFRP tube away from the column ends and generally involving the column mid-height region (Fig. 6). There is also a small difference in the failure mode between the two series of specimens: the concrete in the failure region in Series II specimens was crushed into smaller pieces than that in Series I specimens (Fig. 6). The key experimental results, including the compressive strength f'_{cc}, the ultimate axial strain ε_{cc}, and the FRP hoop rupture strain $\varepsilon_{h,rup}$ of all the FRP-confined concrete columns are summarized in Table 4. In the present paper, compressive stresses and strains in concrete are taken to be positive, while tensile stresses and strains in FRP tubes are taken to be positive unless otherwise specified. The ultimate axial strains were obtained from the mid-height LVDT readings. The axial strains from axial strain gauges are not reported as they are deemed to be not so reliable due to the local buckling/wrinkling of the FRP tube [28,29]. The average FRP hoop rupture strains $\varepsilon_{h,rup}$ were obtained from the readings of the five hoop strain gauges located outside the overlapping zone at the ultimate state (i.e., when FRP tube ruptured) (Fig. 3a). The axial stress of the confined concrete is calculated as the load it takes divided by its cross-sectional area (i.e., ignoring the small axial resistance and cross-sectional area of the FRP tube).

Fig. 7 shows the FRP hoop rupture strains of columns with various RCL mix ratios. The FRP hoop rupture strains were obtained

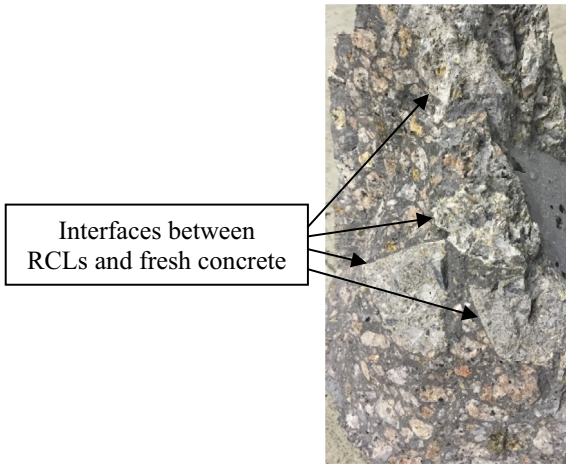

Fig. 5. Surface of fracture of an unconfined compound concrete specimen.

from readings of the five hoop strain gauges outside the overlapping zone. It is obvious that the hoop rupture strain readings exhibit considerable scatters even for two duplicate specimens. The differences between duplicate specimens can be attributed mainly to the randomly non-uniform distribution of RCLs in the concrete, leading to different distributions of hoop strains in the FRP tube in the two duplicate specimens. The RCLs close to the FRP tube are expected to have caused great stress concentrations and premature FRP tube rupture. The inclusion of RCLs, however, does not seem to have an obvious effect on the FRP hoop rupture strains. Instead, the specimens with a higher compressive strength of fresh concrete appears to have a smaller FRP hoop rupture strain as shown in Fig. 7. The negative effect of concrete strength on FRP rupture strains has also been observed by other researchers on normal concrete columns confined with FRP [23,28,30]. Moreover, it can be seen that the specimens with a higher compressive strength of fresh concrete (Series II) generally showed a larger scatter in the FRP hoop strain at rupture around the column circumference. This is mainly attributed to the larger strength difference between the fresh concrete and the RCLs in these specimens, leading to a greater degree of non-uniformity in the compound concrete. Additionally, it is known that a higher strength concrete tends to have more non-uniform deformation after cracking due to its brittleness [30–32]. Zhang et al. [30] also found that the scatter in the FRP hoop strain at rupture around the column circumference became larger for a higher-strength concrete in their normal concrete-filled FRP tubes under axial compression. Fig. 7 also shows that the scatter in the FRP hoop strain at rupture seems to be slightly reduced when the FRP confinement level is increased, which implies that the non-uniform deformation of compound concrete may be reduced through stronger FRP confinement.

3.2. Stress-strain curves

Fig. 8a and 8b show the stress-strain curves of the unconfined concrete specimens with different RCL mix ratios in Series I and Series II, respectively. Again, the mid-height LVDTs were used to obtain the axial strains and the five hoop strain gauges outside

(a) C40-R15-T2 (b) C40-R15-T3-1 (c) C40-R30-T2 (d) C40-R30-T3-1

(e) C60-R15-T2-1 (f) C60-R15-T3-1 (g) C60-R30-T2-1 (h) C60-R30-T3-1

Fig. 6. FCCC columns after test.

Table 4
Key experimental results of CCFFT columns.

Series	Specimen	f'_{cc} (MPa)	Average f'_{cc} (MPa)	ε_{cc}	Average ε_{cc}	$\varepsilon_{h,rup}$	Average $\varepsilon_{h,rup}$
Series I	C40-R0-T2	79.7	79.7	0.0240	0.0240	0.0156	0.0156
	C40-R15-T2	79.0	79.0	0.0224	0.0224	0.0154	0.0154
	C40-R30-T2	80.2	80.2	0.0225	0.0225	0.0156	0.0156
	C40-R0-T3-1	98.0	104.0	0.0304	0.0308	0.0156	0.0162
	C40-R0-T3-2	109.6		0.0312		0.0168	
	C40-R15-T3-1	105.7	102.3	0.0308	0.0275	0.0160	0.0147
	C40-R15-T3-2	99.0		0.0241		0.0134	
	C40-R30-T3-1	91.5	97.6	0.0212	0.0237	0.0110	0.0128
	C40-R30-T3-2	103.8		0.0261		0.0145	
Series II	C60-R0-T2-1	99.5	96.7	0.0164	0.0153	0.0137	0.0135
	C60-R0-T2-2	93.8		0.0142		0.0133	
	C60-R15-T2-1	86.3	90.6	0.0133	0.0138	0.0122	0.0130
	C60-R15-T2-2	94.9		0.0143		0.0137	
	C60-R30-T2-1	89.8	92.0	0.0128	0.0136	0.0143	0.0140
	C60-R30-T2-2	94.2		0.0143		0.0137	
	C60-R0-T3-1	119.5	116.5	0.0175	0.0168	0.0148	0.0140
	C60-R0-T3-2	113.5		0.0161		0.0131	
	C60-R15-T3-1	121.3	120.8	0.0195	0.0198	0.0149	0.0145
	C60-R15-T3-2	120.3		0.0200		0.0141	
	C60-R30-T3-1	120.4	117.9	0.0208	0.0193	0.0166	0.0153
	C60-R30-T3-2	115.3		0.0178		0.0140	

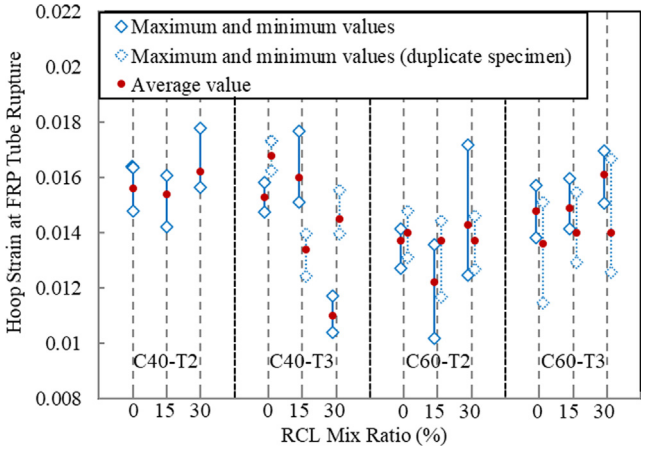

Fig. 7. Hoop strains at FRP tube rupture of FCCC columns.

the overlapping zone were used to obtain the hoop strains. For some specimens (e.g., C60-R30-T0-2 and C40-R30-T0-2), some of the hoop strain gauges were damaged before the attainment of the maximum axial strain; thus the axial stress-hoop/lateral strain curve terminates slightly earlier than the corresponding axial stress-axial strain curve. It is obvious that the inclusion of RCLs affects considerably the axial stress-strain curve, especially after the initial portion, of unconfined concrete. The peak axial stress becomes significantly smaller for a larger RCL mix ratio. It is also seen that the inclusion of RCLs does not significantly affect the axial strain at peak stress for Series I specimens; however, the axial strain at peak stress also becomes smaller as the RCL mix ratio increases for Series II specimens (Table 3).

The axial stress-axial strain curves and axial stress-lateral strain curves of all the FRP-confined concrete column specimens are shown in Fig. 9. The stress-strain curves feature the well-known bilinear shape with an ascending second branch. The specimens containing RCLs have stress-strain curves very close to those of the corresponding normal concrete specimens without RCLs; the differences between the two are much smaller than those observed for the unconfined concrete specimens (Fig. 8). These results demonstrate that, with a strong level of lateral confinement exerted by the CFRP tube, the detrimental effect of the interfaces between the fresh concrete and the RCLs is substantially reduced. Nevertheless, the presence of RCLs indeed has a small effect on the stress-strain behavior of FRP-confined compound concrete. For Series I specimens confined with a 2-ply CFRP tube, the axial stresses of specimens containing RCLs at the transition between

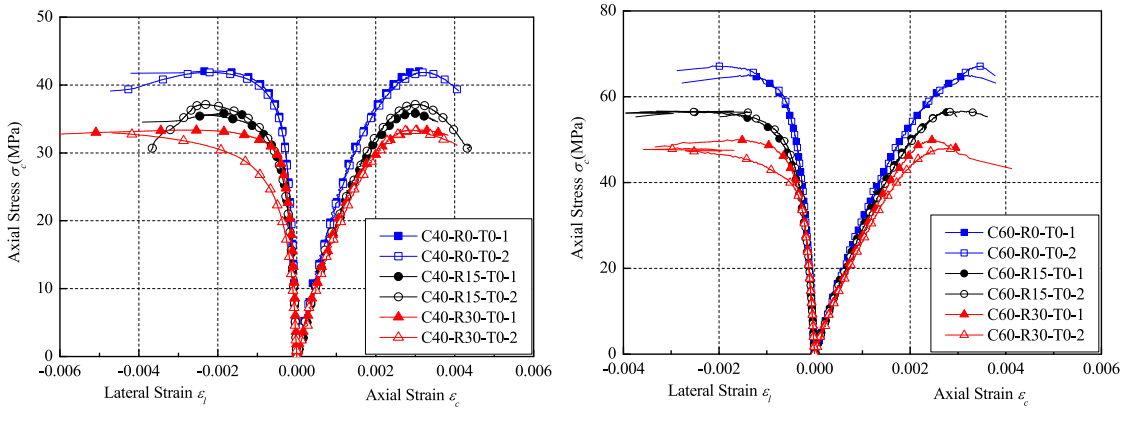

(a) Series I (b) Series II

Fig. 8. Stress-strain curves of unconfined concrete specimens.

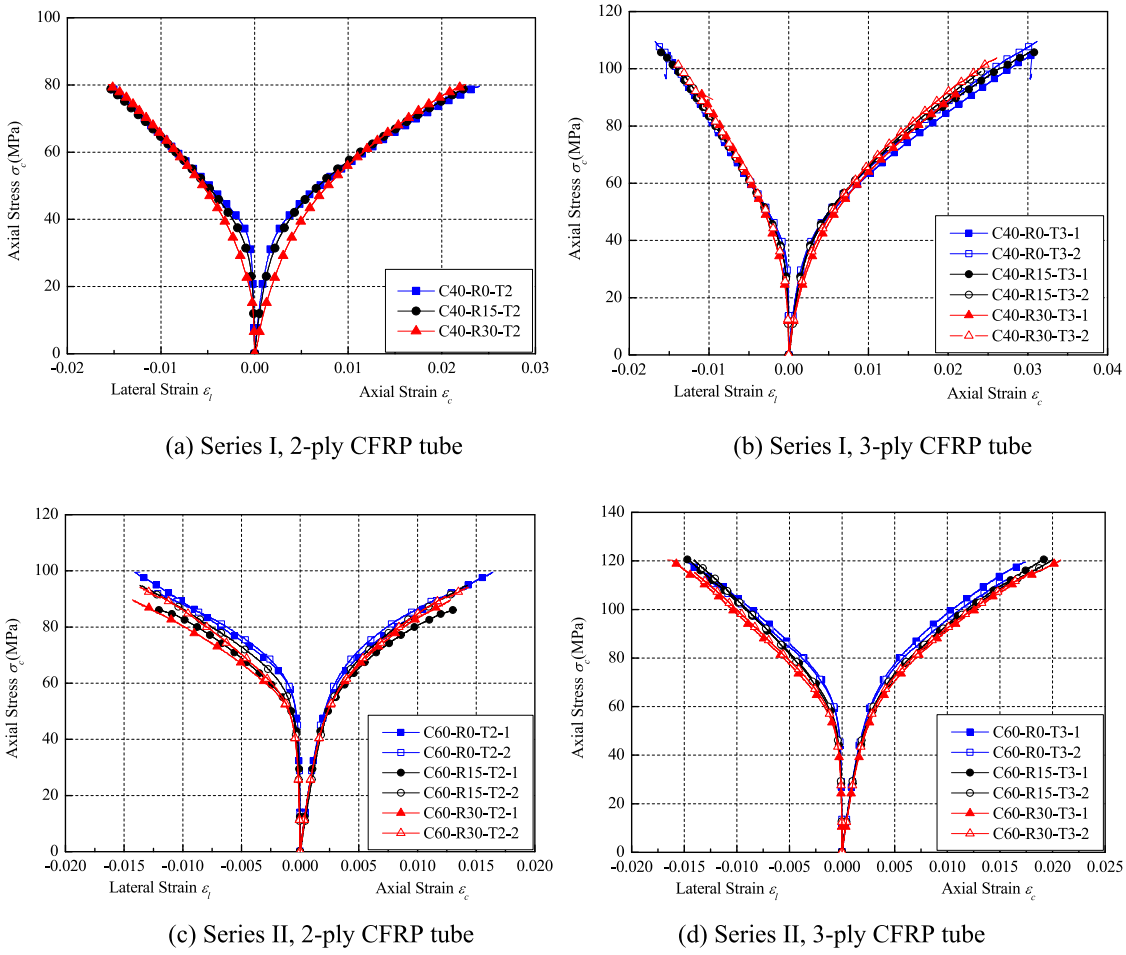

(a) Series I, 2-ply CFRP tube

(b) Series I, 3-ply CFRP tube

(c) Series II, 2-ply CFRP tube

(d) Series II, 3-ply CFRP tube

Fig. 9. Stress-strain curves of FRP-confined concrete columns.

the two branches of the stress-strain curve are smaller than those of the specimens without RCLs, but they become close to each other when the axial strain exceeds about 0.01 (Fig. 9a). Similar observations have been reported by Teng et al. [14] for compound concrete filled filament-wound GFRP tubes. However, this phenomenon becomes less obvious for specimens confined with a thicker FRP tube (see Fig. 9b). For Series II specimens, the transition portion and the second ascending branch of a specimen containing RCLs are only slightly lower than those of the corresponding specimen without RCLs (Fig. 9c and d).

The influence of the FRP confinement level (i.e., FRP tube thickness) on the stress-strain behavior of FRP-confined compound concrete is shown in Fig. 10. It is evident that the ultimate stress and the ultimate strains of FRP-confined concrete are much larger than those of the corresponding unconfined concrete, and both the ultimate stress and the ultimate strains increase as the FRP confinement level increases. In addition, the stress-strain curves of two duplicate specimens of each pair are generally very close to each other except for the ultimate strains of specimens C40-R15-T3-1,2 and C40-R30-T3-1,2 in Series I. The differences observed for these two pairs of nominally identical specimens can be attributed mainly to the randomly non-uniform distribution of RCLs in the concrete core as mentioned earlier.

3.3. Axial strain-lateral strain curves

Fig. 11 shows the axial strain-lateral strain curves of concrete in all the FRP-confined concrete specimens. It can be seen that the specimens with the same FRP confinement displayed very similar axial strain-lateral strain curves regardless of the RCL mix ratio (except for specimen C60-R30-T2-2 whose lateral strains are unreasonably large in magnitude compared with other specimens). This observation also implies that the inclusion of RCLs has a very limited effect on the dilation behavior of FRP-confined concrete in the test specimens.

4. Theoretical analysis

4.1. Jiang and Teng's model [25]

Jiang and Teng's model [25], a well-known analysis-oriented stress–strain model, has been shown to be one of the most successful models for FRP-confined normal concrete [33,34]. The predictions of this model are compared with the experimental results in the present study. In this model, a stress-strain model for actively confined concrete forms one of the key elements. The following stress-strain relationship of Popovics [35] for actively confined concrete is employed:

$$\frac{\sigma_c}{f'^{*}_{cc}} = \frac{(\varepsilon_c/\varepsilon^{*}_{cc})r}{r-1+(\varepsilon_c/\varepsilon^{*}_{cc})^{r}} \tag{1}$$

$$r = \frac{E_c}{E_c - f'^{*}_{cc}/\varepsilon^{*}_{cc}} \tag{2}$$

where σ_c and ε_c = axial stress and corresponding axial strain of concrete. The peak axial stress f'^{*}_{cc} and the axial strain at peak

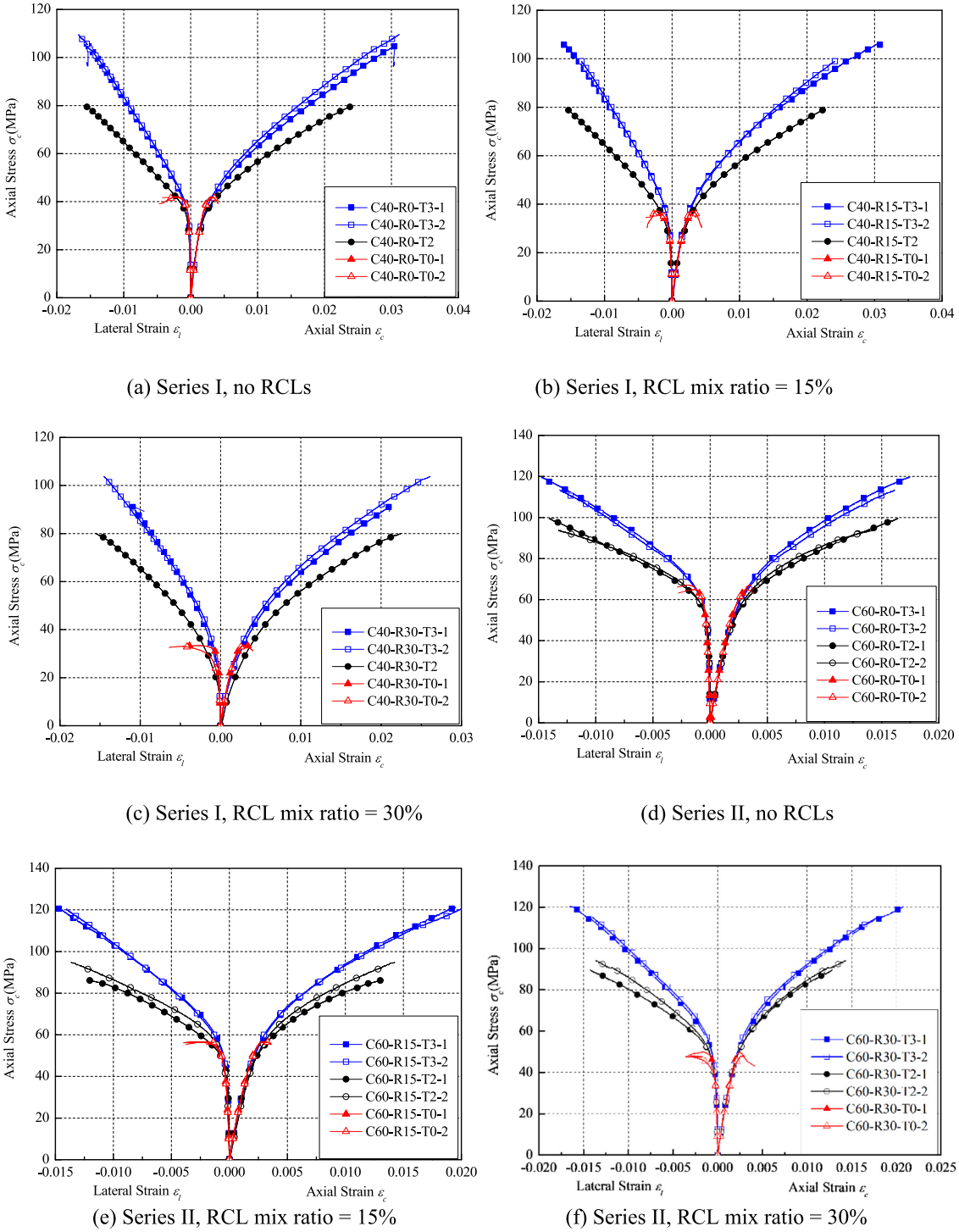

(a) Series I, no RCLs

(b) Series I, RCL mix ratio = 15%

(c) Series I, RCL mix ratio = 30%

(d) Series II, no RCLs

(e) Series II, RCL mix ratio = 15%

(f) Series II, RCL mix ratio = 30%

Fig. 10. Effect of CFRP tube thickness on stress-strain response.

stress ε_{cc}^{*} of concrete under a constant confining pressure σ_l in Jiang and Teng's model [25] are calculated using the following equations:

$$\frac{f_{cc}'^{*}}{f_{co}'} = 1 + 3.5\frac{\sigma_l}{f_{co}'} \tag{3}$$

$$\frac{\varepsilon_{cc}^{*}}{\varepsilon_{co}} = 1 + 17.5\left(\frac{\sigma_l}{f_{co}'}\right)^{1.2} \tag{4}$$

In the above equations, the confining pressure σ_l is given by:

$$\sigma_l = \frac{2E_{frp}t\varepsilon_h}{d} = -\frac{2E_{frp}t\varepsilon_l}{d} \tag{5}$$

where E_{frp} and t = FRP tube hoop elastic modulus and thickness; ε_h = FRP hoop strain; $\varepsilon_l = -\varepsilon_h$ = lateral strain of concrete; and d = diameter of confined concrete core.

Another key element in Jiang and Teng's model [25] is the equation for the axial strain-hoop strain relationship, which takes the following form as initially proposed by Teng et al. [36]:

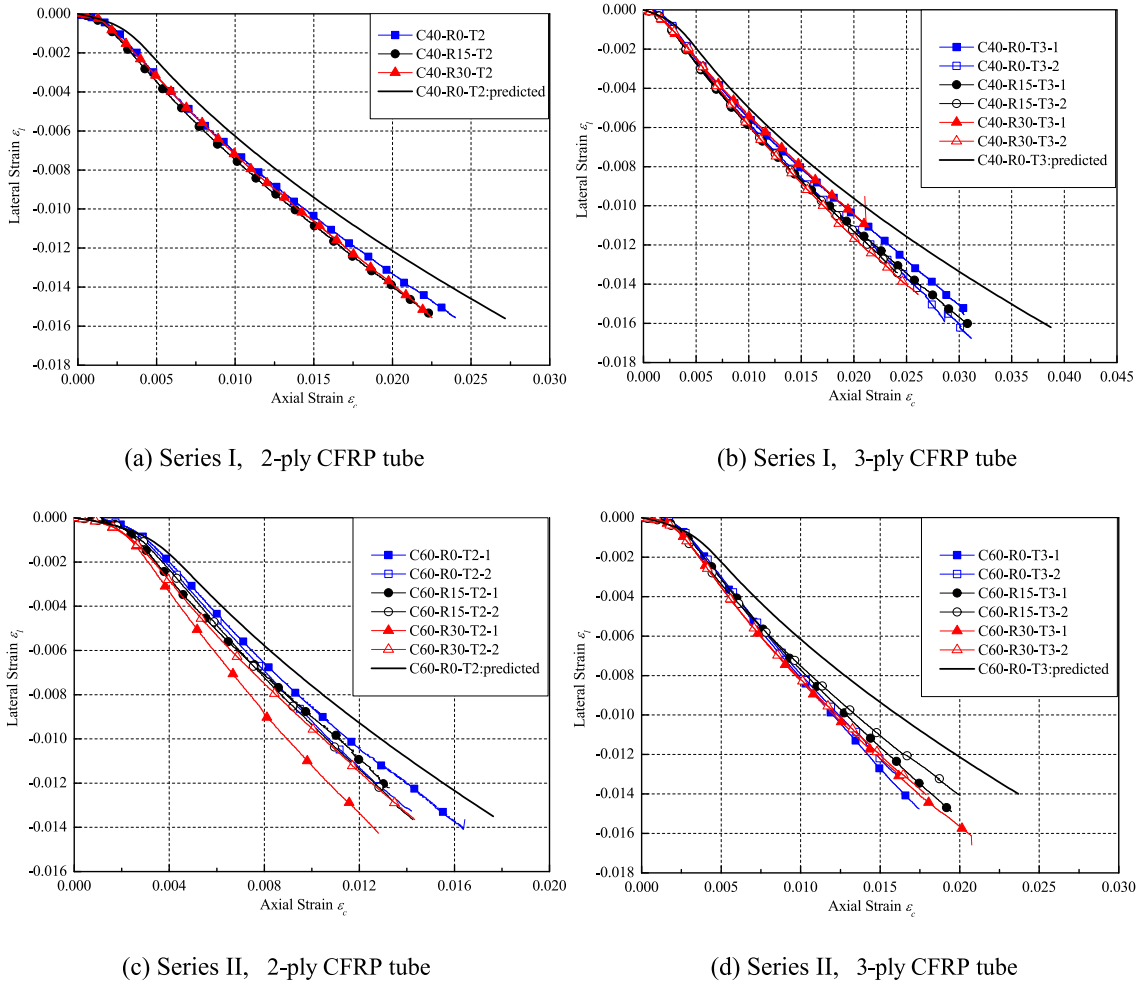

(a) Series I, 2-ply CFRP tube

(b) Series I, 3-ply CFRP tube

(c) Series II, 2-ply CFRP tube

(d) Series II, 3-ply CFRP tube

Fig. 11. Axial strain-lateral strain curves of FRP-confined concrete columns.

$$\frac{\varepsilon_c}{\varepsilon_{co}} = 0.85\left(1+8\frac{\sigma_l}{f'_{co}}\right)\times\left\{\left[1+0.75\left(\frac{\varepsilon_h}{\varepsilon_{co}}\right)\right]^{0.7}-\exp\left[-7\left(\frac{\varepsilon_h}{\varepsilon_{co}}\right)\right]\right\} \quad (6)$$

4.2. Comparisons and discussions

The predicted axial strain-lateral strain curves and axial stress-strain curves are compared with the experimental results in Figs. 11 and 12, respectively. The compressive strength of fresh concrete obtained from the unconfined concrete specimens without RCLs (Fig. 8) was used in making the predictions since RCLs had only a small effect on the stress-strain behavior of FRP-confined compound concrete (see Fig. 9). The experimental FRP hoop rupture strain averaged from two duplicate specimens without RCLs was used to determine the ultimate condition (i.e., ultimate axial stress/strain) of the corresponding specimens with RCLs (Table 4). Fig. 12 shows that Jiang and Teng's model [25] predicts reasonably well the behavior of all specimens, except for the late loading stage of Series I specimens confined with a three-ply CFRP tube, for which the slope of the second ascending branch is underestimated by the model (Fig. 12b). Note that the confinement ratios (σ_l/f'_{co}) of these specimens are larger than 0.3 when the axial strain exceeds around 0.02. The confinement ratios in the test database to derive Eq. (3) in Jiang and Teng's [25] model, however, are smaller than 0.3. This observation suggests that Jiang and Teng's [25] model may need to be refined for more accurate predictions of concrete with a high level of FRP confinement.

It is worth noting that the second branch slopes of the axial stress-axial strain curves of all the FRP-confined concrete specimens tested by Teng et al. [14] are significantly underestimated by Jiang and Teng's model [25]. The different observations about the test results in the two studies are attributed mainly to the use of two different types of FRP tubes: filament-wound FRP tubes with a significant axial stiffness in Teng et al.'s [14] study and wet-layup FRP tubes with a negligible axial stiffness in the present study.

5. Conclusions

Compared with the recycling of demolition concrete into coarse aggregate, the use of recycled concrete lumps (RCLs) for direct mixing with fresh concrete, leading to what is herein referred to as compound concrete, has obvious advantages in efficiency, cost-effectiveness and recycling ratio. Encasement of compound concrete with an FRP confining tube has recently been explored as an effective means to improve the mechanical properties and durability of compound concrete. This paper has presented the results of an experimental program on the stress-strain behavior of FRP-confined compound concrete in which CFRP confining tubes which fibers oriented only in the hoop direction were used to provide confinement. The effects of RCL mix ratio, strength difference

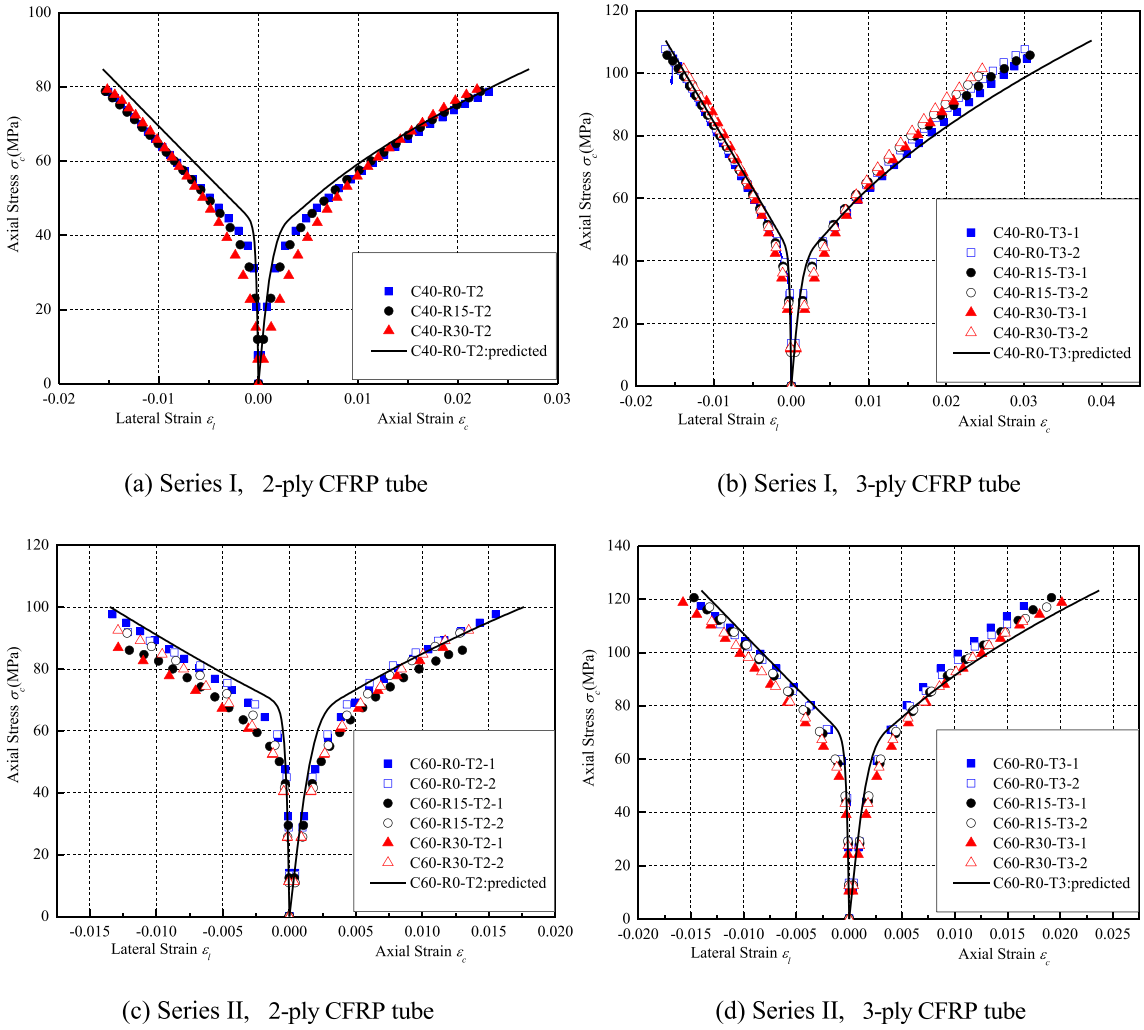

(a) Series I, 2-ply CFRP tube

(b) Series I, 3-ply CFRP tube

(c) Series II, 2-ply CFRP tube

(d) Series II, 3-ply CFRP tube

Fig. 12. Comparison of stress-strain curves between tests and Jiang and Teng's model.

between the RCLs and the fresh concrete, and CFRP tube thickness have been examined. The following observations and conclusions may be drawn:

(1) The failure mode of unconfined compound concrete column specimens was similar to that of normal concrete column specimens. The inclusion of RCLs significantly reduced the compressive strength and the initial elastic modulus of unconfined concrete, and the reduction increased with the RCL mix ratio.
(2) Except for the two FCCC columns with an outdated resin in the CFRP tube, all the FCCC columns failed by FRP rupture due to hoop tension, and the presence of RCLs did not have an obvious effect on the column failure mode.
(3) FRP confinement can significantly enhance the performance of compound concrete: the compressive strength and the ultimate axial strain of compound concrete are comparable to those of the corresponding fresh concrete (i.e., without the presence of RCLs) under the same level of FRP confinement, which indicates that the detrimental effects caused by the use of RCLs in unconfined concrete can be largely eliminated by FRP confinement.
(4) The axial stress-strain behaviors of confined concrete in the test specimens with different RCL mix ratios are close to each other, implying that the inclusion of RCLs may have a limited influence on the confinement mechanism in FRP-confined concrete. However, more research on FRP-confined compound concrete with wider ranges of parameters (e.g., RCL mix ratio and FRP confinement level) is needed for a deeper understanding of the confinement mechanism in FRP-confined compound concrete.
(5) Jiang and Teng's model [25] generally predicts reasonably well the axial stress-strain curves of FRP-confined concrete in all specimens in the present study; however, the second branch slopes of all the specimens tested by Teng et al. [14] were significantly underestimated by Jiang and Teng's model [25]. This difference is believed to be attributed to the much smaller axial stiffnesses of the FRP tubes used in the present study than those of the filament-wound FRP tubes used in Teng et al.'s [14] study.

The above conclusions reveal that most of the weaknesses of compound concrete containing RCLs can be minimized through the provision of FRP confinement. In addition, the use of an FRP tube eliminates the corrosion concern for the internal steel reinforcement (if it is present) due to the premature cracks between RCLs and fresh concrete. It is also worth noting that, while CFRP tubes with fibers oriented in the hoop direction only were used in the present study (as the main purpose was to clearly reveal the stress-strain behavior of FRP-confined compound concrete),

filament-wound GFRP tubes, which are more cost-effective than CFRP tubes, should be used in practice. The combination of GFRP tubes with compound concrete opens many possibilities for the reliable use of compound concrete in new construction and offers a reliable and cost-effective way of using recycled demolition concrete.

CRediT authorship contribution statement

J.K. Zhou: Methodology, Investigation, Formal analysis, Visualization, Writing - original draft. **Guan Lin:** Methodology, Investigation, Supervision, Visualization, Writing - review & editing. **J.G. Teng:** Conceptualization, Methodology, Supervision, Visualization, Writing - review & editing, Funding acquisition.

Declaration of Competing Interest

The authors declare that they have no known competing financial interests or personal relationships that could have appeared to influence the work reported in this paper.

Acknowledgements

The authors are grateful for the financial support received from the National Key R&D Program of China (Project No. 2017YFC0703000), the Research Grants Council of the Hong Kong Special Administrative Region (Project Reference Number: PolyU 5252/13E), and The Hong Kong Polytechnic University (Project Account Code: 1-BBAG).

References

[1] T.C. Hansen, Recycled aggregates and recycled aggregate concrete second state-of-the-art report developments 1945–1985, Mater. Struct. 19 (3) (1986) 201–246.
[2] N.F. Günçan, Using waste concrete as aggregate, Cem. Concr. Res. 25 (7) (1995) 1385–1390.
[3] C.S. Poon, Z.H. Shui, L. Lam, Effect of microstructure of ITZ on compressive strength of concrete prepared with recycled aggregates, Constr. Build. Mater. 18 (6) (2004) 461–468.
[4] J. Xiao, J. Li, C.h. Zhang, Mechanical properties of recycled aggregate concrete under uniaxial loading, Cem. Concr. Res. 35 (6) (2005) 1187–1194.
[5] Z.H. Duan, C.S. Poon, Properties of recycled aggregate concrete made with recycled aggregates with different amounts of old adhered mortars, Mater. Des. 58 (2014) 19–29.
[6] V.W.Y. Tam, M. Soomro, A.C.J. Evangelista, A review of recycled aggregate in concrete applications (2000–2017), Constr. Build. Mater. 172 (2018) 272–292.
[7] J. Pacheco, J. de Brito, C. Chastre, L. Evangelista, Experimental investigation on the variability of the main mechanical properties of recycled aggregate concrete, Constr. Build. Mater. 201 (2019) 110–120.
[8] B. Lu, C. Shi, Z. Cao, M. Guo, J. Zheng, Effect of carbonated coarse recycled concrete aggregate on the properties and microstructure of recycled concrete, J. Cleaner Prod. 233 (2019) 421–428.
[9] B.J. Zhan, D.X. Xuan, W. Zeng, C.S. Poon, Carbonation treatment of recycled concrete aggregate: effect on transport properties and steel corrosion of recycled aggregate concrete, Cem. Concr. Compos. 104 (2019) 103360.
[10] J. Bao, S. Li, P. Zhang, X. Ding, S. Xue, Y. Cui, T. Zhao, Influence of the incorporation of recycled coarse aggregate on water absorption and chloride penetration into concrete, Constr. Build. Mater. 239 (2020) 117845.
[11] Y.-F. Yang, L.-H. Han, Experimental behaviour of recycled aggregate concrete filled steel tubular columns, J. Constr. Steel Res. 62 (12) (2006) 1310–1324.
[12] B. Wu, Q.X. Liu, W. Liu, Z. Xu, Primary study on recycled-concrete-segment filled steel tubular members, Earthq. Resistant Eng. Retrof. 30 (2008) 120–124 (in Chinese).
[13] J.G. Teng, J.L. Zhao, T. Yu, l.J. Li, Y.C. Guo, Recycling of coarsely-crushed concrete for use in FRP tubular columns. Proceedings of the 1st International Conference on Performance-based and Life-cycle Structural Engineering (PLSE 2012), 2012.
[14] J.G. Teng, J.L. Zhao, T. Yu, L.J. Li, Y.C. Guo, Behavior of FRP-confined compound concrete containing recycled concrete lumps, J. Compos. Constr. 20 (1) (2016) 04015038, https://doi.org/10.1061/(ASCE)CC.1943-5614.0000602.
[15] B.o. Wu, C. Liu, Y. Wu, Compressive behaviors of cylindrical concrete specimens made of demolished concrete blocks and fresh concrete, Constr. Build. Mater. 53 (2014) 118–130.
[16] B.o. Wu, S. Zhang, Y. Yang, Compressive behaviors of cubes and cylinders made of normal-strength demolished concrete blocks and high-strength fresh concrete, Constr. Build. Mater. 78 (2015) 342–353.
[17] B. Wu, Q. Zhang, G.M. Chen, Compressive behavior of thin-walled circular steel tubular columns filled with steel stirrup-reinforced compound concrete, Eng. Struct. 170 (2018) 178–195.
[18] B.o. Wu, W.-F. Li, X.-Y. Zhao, Behavior of slender square steel tubular columns filled with fresh concrete and demolished concrete lumps, Procedia Eng. 210 (2017) 196–202.
[19] B.o. Wu, X.-Y. Zhao, J.-S. Zhang, Cyclic behavior of thin-walled square steel tubular columns filled with demolished concrete lumps and fresh concrete, J. Constr. Steel Res. 77 (2012) 69–81.
[20] B.o. Wu, L. Lin, J. Zhao, H. Yan, Creep behavior of thin-walled circular steel tubular columns filled with demolished concrete lumps and fresh concrete, Constr. Build. Mater. 187 (2018) 773–790.
[21] B. Wu, X.Y. Zhao, Y. Yang, Regeneration structural members containing large-size demolished concrete: a review, J. South China Univ. Technol. (Nat. Sci. Ed.) 40 (2012) 174–183 (in Chinese).
[22] X.-Y. Zhao, B.o. Wu, L. Wang, Structural response of thin-walled circular steel tubular columns filled with demolished concrete lumps and fresh concrete, Constr. Build. Mater. 129 (2016) 216–242.
[23] J.G. Teng, J.F. Chen, S.T. Smith, L. Lam, FRP Strengthened RC Structures, Wiley, West Sussex, UK, 2002.
[24] G. Lin, Seismic Performance of FRP-Confined RC Columns: Stress-Strain Models and Numerical Simulation [PhD Thesis], The Hong Kong Polytechnic University, Hong Kong, China, 2016.
[25] T. Jiang, J.G. Teng, Analysis-oriented stress–strain models for FRP–confined concrete, Eng. Struct. 29 (11) (2007) 2968–2986.
[26] BS 812. Testing of Aggregate Part 2: Method of Determination of Density. British Standards Institution London, UK, 1995.
[27] ASTM D3039. Standard Test Method for Tensile Properties of Ploymer Matrix Composite Materials. American Society for Testing and Materials, West Conshohocken, USA, 2008.
[28] T. Vincent, T. Ozbakkaloglu, Influence of concrete strength and confinement method on axial compressive behavior of FRP confined high- and ultra high-strength concrete, Compos. B Eng. 50 (2013) 413–428.
[29] J.Y. Zhu, G. Lin, J.G. Teng, T.M. Chan, J.J. Zeng, L.J. Li, FRP-confined square concrete columns with section curvilinearization under axial compression, J. Comp. Constr. 24 (2020) 04020004.
[30] B. Zhang, T. Yu, J.G. Teng, Behavior of concrete-filled FRP tubes under cyclic axial compression, J. Comp. Constr. 19 (2015) 04014060.
[31] J.C. Lim, T. Ozbakkaloglu, Hoop strains in FRP-confined concrete columns: experimental observations, Mater. Struct. 48 (9) (2015) 2839–2854.
[32] Q.G. Xiao, J.G. Teng, T. Yu, Behavior and modeling of confined high-strength concrete, J. Comp. Constr. 14 (2010) 249–259.
[33] C.-S. Lee, G.A. Hegemier, Model of FRP-confined concrete cylinders in axial compression, J. Compos. Constr. 13 (5) (2009) 442–454.
[34] T. Ozbakkaloglu, J.C. Lim, T. Vincent, FRP-confined concrete in circular sections: review and assessment of stress–strain models, Eng. Struct. 49 (2013) 1068–1088.
[35] S. Popovics, A numerical approach to the complete stress-strain curve of concrete, Cem. Concr. Res. 3 (5) (1973) 583–599.
[36] J.G. Teng, Y.L. Huang, L. Lam, L.P. Ye, Theoretical model for fiber-reinforced polymer-confined concrete, J. Comp. Constr. 11 (2007) 201–210.
[37] P. Xie, G. Lin, J.G. Teng, T. Jiang, Modelling of concrete-filled filament-wound FRP confining tubes considering nonlinear biaxial tube behavior, Eng. Struct. 218 (2020) 110762.